Spring 2022

Austenitic, Duplex, and Lean Duplex Stainless Steel Critical Pitting Temperature in Simulated Concrete Environment

Bobby Giebel
rag81@uakron.edu

Recommended Citation

Giebel, Bobby, "Austenitic, Duplex, and Lean Duplex Stainless Steel Critical Pitting Temperature in Simulated Concrete Environment" (2022). *Williams Honors College, Honors Research Projects*. 1542. https://ideaexchange.uakron.edu/honors_research_projects/1542

Austenitic, Duplex, and Lean Duplex Stainless Steel Critical Pitting Temperature in Simulated Concrete Environment

Robert Giebel

Department of Chemical, Biomolecular, and Corrosion Engineering

Honors Research Project

Submitted to

The University of Akron Williams Honors College

Academic Supervision: Dr. David M. Bastidas and Ulises Martin Diaz
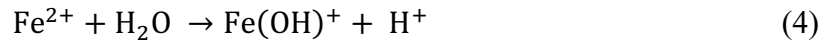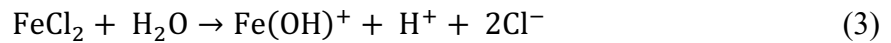
Spring 2022

Table of Contents

1. ABSTRACT

In this work, the critical pitting temperature (CPT) will be observed for a selection of austenitic (316LN and 24100) and duplex (2205), and lean duplex (2304, 2001) stainless steels in simulated concrete pore solution. To study the influence of temperature on the pitting stability of the stainless steels, three temperatures were tested: 25°C, 45°C, and 65°C for cyclic potentiodynamic polarization (CPP) and electrochemical impedance spectroscopy (EIS). Electrochemical properties of the interfaces we studied via EIS analysis. Kinetics were studied via CPP testing. To reveal the critical pitting temperature of the stainless steels, cyclic thermammetry was used. Characterization of the pits was studied via, OM, IFM, and SEM.

2. INTRODUCTION

When it comes to categorizing corrosion, there are two main genres in which it can be classified. The divide is in uniform corrosion versus localized corrosion. Uniform corrosion is the simultaneous oxidation of the entirety of a metallic surface. On the contrary is the phenomena of localized corrosion, more specifically pitting corrosion. Pitting corrosion is commonly experienced in metals that form a passive film or have a coating applied to them. Any defects in the film can lead to concentrated attack by a corrosive specifies on the bare metal, which results in rapid and detrimental corrosion at those defective areas. This is known as pitting corrosion.

Pitting of stainless steel is heavily influenced by chloride concentration and has been a popularly studied environmental factor [10-14]. Chloride ions will depassivate the stainless steel and locally accelerate the dissolution of the metal ions. When this occurs, H+ ions are produce to create local acidification. The full chemical reactions for local acidification are outline in **Equation 1-4**. The increase of protons in this area decreases the pH, down to 3 at times, hence the

term local acidification. Steels can withstand a certain amount of chloride before corrosion occurs, known as the chloride threshold. Generally, stainless steels can withstand up to 8% - 12% chlorides, which is well above that of carbon steel, around 3%. Additionally, the corrosion behaviour of each type of steel varies when exposed to chloride. Stainless steels will experience localized corrosion, such as pitting, while carbon steels will see uniform corrosion across the surface due to the lower corrosion protection compared to stainless steel [13].

$$Fe \rightarrow Fe^{2+} + 2e^- \tag{1}$$
$$Fe^{2+} + 2Cl^- \rightarrow FeCl_2 \tag{2}$$
$$FeCl_2 + H_2O \rightarrow Fe(OH)^+ + H^+ + 2Cl^- \tag{3}$$
$$Fe^{2+} + H_2O \rightarrow Fe(OH)^+ + H^+ \tag{4}$$

However, when stainless steel is placed into a concrete environment, the chloride threshold falls to 4.9wt% Chlorides. This was found in study using ANSI 316LN stainless steel [14,15]. In a concrete environment, where pH is generally very high, stainless steel reinforcements still have a higher chloride threshold than carbon steel.

An observable parameter of pitting corrosion is the CPT of a material for a given environment. Generally, as temperature of an environment surrounding a material is raised, so is the likeliness of pitting corrosion occurring, due to the higher activation of the chlorides with increasing temperature. Pitting in a given environment, containing a specific pH and concentration of chlorides, will not occur in a material until a critical temperature is achieved by the environment. In other words, there is a minimum temperature that is material specific in which the initiation of pitting corrosion will occur, this is known as the alloy CPT.

Throughout a series of tests, the objective of this experiment is to determine the critical pitting temperature of five different alloys in simulated concrete pore solution including: austenitic, duplex and lean duplex stainless-steel. Each of these alloys have been studied as alternatives for steel rebar in reinforced concrete applications. Having a sound understanding of its critical pitting temperature, along with other corrosion and mechanical properties, is crucial for material selection when creating rebar supported concrete.

3. EXPERIMENTAL

The materials used for the CPT study were austenitic 316LN and 24100 along with duplex 2205, and lean duplex 2304, and 2001. Each respective elemental composition can be seen in **Table 1**, along with Pitting Resistance Equivalent Number (PREN), Nickel equivalent weight and Chromium equivalent weight. The PREN can be easily calculated with **Equation 5** using information from a given materials composition [16,17]. In this study, the highest PREN belonged to duplex 2205 and the lowest belonged to austenitic 24100.

$$PREN = wt.\% \ Cr + 3.3 \ (wt.\% \ Mo) + 16 \ (wt.\% \ N) \tag{5}$$

The PREN is a parameter useful in determining the resistance to local pitting corrosion in stainless steels. If a PREN is below 30, it suggests that the material has low susceptibility to pitting corrosion. This is why stainless steels rich in Chromium and Nitrogen have good resistance to pitting corrosion [18].

For austenitic stainless steels, their material composition generally allows them to have face centered cubic crystal structure, a pure γ–phase matrix. This is due to high concentrations of chromium, nickel, manganese, among others, allows for high Ni-equivalent and Cr-equivalent

numbers, which in turn promotes the γ–phase matrix. The Ni-equivalent and Cr-equivalent numbers can be easily calculated via **Equation 6 and 7** respectively.

$$\text{Ni-equivalent} = \text{Ni} + 30 \times \text{C} + 0.5 \times \text{Mn} \tag{6}$$

$$\text{Cr-equivalent} = \text{Cr} + \text{Mo} + 1.5 \times \text{Si} + 0.5 \times \text{Nb} + 2 \times \text{Ti} \tag{7}$$

Higher Ni-equivalent and Cr-equivalent values correlate to greater resistance to corrosion.

Table 1 elemental composition, PREN, Nickel equivalent weight and Chromium equivalent weight of austenitic, duplex, and lean duplex stainless steel

Alloy	C %	Cr %	Mn %	N %	Ni %	P %	S %	Si %	Co %	Mo %	Cu %	Fe %	PREN	Ni-equiv	Cr-equiv
316LN	0.016	17.55	1.18	0.167	10.1	0.03	0.001	0.25	0	2.12	0	68.586	27.22	11.17	20.05
24100	0.078	18.21	12.72	0.277	0.92	0.023	0.0038	0.77	0	0	0	66.9982	22.64	9.62	19.37
2205	0.017	22.76	1.57	0.171	4.64	0.024	0.002	0.34	0.17	3.21	0	67.096	36.09	5.94	26.48
2304	0.013	22.57	1.64	0.161	4.03	0.03	0.0006	0.46	0.09	0.18	0.32	70.5054	25.74	5.24	23.44
2001	0.028	20.07	4.19	0.129	1.78	0.023	0.01	0.65	0	0.22	0.08	72.82	22.86	4.72	21.27

Each of the samples were mounted and polished to 1200 SiC to reduce surface roughness and obtain consistent surface condition across all samples. Experimental began with EIS testing for each alloy at 25°C, 45°C, and 65°C. Additionally, in order to observe temperature effect on the pitting initiation, the pitting potential was first experimentally determined for each alloy at 25°C, 45°C, and 65°C via CPP in simulated concrete pore solution.

Following ASTM G150-18, 1.0M NaCl was added to the simulated concrete pore solution to find the CPT of each stainless steel, mimicking the concrete environment in which the steel rebar sits. Per 1.0 L of solution, the creation of this simulated concrete pore solution requires 58.44 g of NaCl and ~2.0 g of $Ca(OH)_2$, which is enough $Ca(OH)_2$ to saturate the solution. The final pH of the solution is 12.6 Once all combined in a flask, the solution is stirred until a homogeneous solution is acquired, then filtered to removed excess $Ca(OH)_2$ solids.

EIS testing is a non-destructive evaluation technique that can be to study the change in electrochemical properties of the interface. The reference electrode for the cell is saturated calomel electrode (SCE), and graphite acts as the counter electrode. After a 60-minute open circuit potential (OCP), EIS tests were conducted for each sample at 25°C, 45°C, and 65°C. Testing parameters for this study ranged from 10^5–10^{-2} Hz and is optimized for the lowest noise as possible [22]. This EIS testing was conducted with an applied 10 mV AC excitation signal and at a step rate of 5 points per decade

After completion of the EIS testing, potentiodynamic testing was done for each of the five alloys. Similarly, the reference electrode for the cell is SCE, and graphite acts as the counter electrode. Initial potential for the test is –0.3 V with a scan rate of 1.667 mV/s, in accordance to ASTM G61-86 [23]. For this test specifically, it is found that turning off IR compensation for the system led to the clearest data. Once completed, pitting potentials are obtained from the data for each of the 15 tests.

The lowest pitting potential (E_{pit}) between the five alloys tested at 65°C was used as the potential in the potentiostatic critical pitting temperature testing. This testing method, known as cyclic thermammetry, begins with the environment at 25 °C and slowly steps up until 80°C is reached. Through this temperature evolution, an obscurity in data will reveal a temperature where pitting began [24]. This is the coveted alloy critical pitting temperature.

Once all electrochemical testing was completed, a series of other evolution methods were used to gain an understanding of the pit formation and chemistry in austenitic, duplex, and lean duplex stainless steels. Imaging of the pits in the form of optical microscopy (OM), infinite focus microscopy (IFM), and scanning electron microscopy (SEM).

4. RESULTS AND DISCUSSION

4.1 Cyclic Potentiodynamic Polarization (CPP)

Electrochemical CPP testing can be used to acquire a variety of parameters from a materials performance in a given environment. Two of these parameters are the corrosion potential (E_{corr}) and the corrosion current density (i_{corr}) [19]. The E_{corr} is the potential in which the metal transitions from cathodic behavior to anodic behavior. A higher E_{corr} generally correlates to less likeliness for corrosion to occur and is identifiable on a CPP graph by the near constant potential that rapidly decreases, then increase in current. In the case of the i_{corr}, this parameter can be converted to corrosion rate. The i_{corr} is found where the two Tafel slopes meet. It often needs the use of a computer software to precisely identify from a CPP graph.

For the stainless steels observed in this study, the E_{corr} and i_{corr} were found for each and the graphical representations are shown in **Figure 1** at 25°C and summarized in **Table 2.** For the austenitic stainless steels, the highest E_{corr} belongs to 316LN with a value of -0.255 V_{OCP} at 25°C. For the duplex and lean duplex steels, the highest E_{corr} belongs to 2205 with a value of -0.213 V_{OCP} at 25°C. These were comparable values, with duplex 2205 having the slightly higher E_{corr}.

Similarly, the i_{corr} values for each of the stainless steels can be compared. For the austenitic stainless steels, the lowest i_{corr} belongs to 316LN with a value of 1.70E-07 A/cm^2 at 25°C. For the duplex and lean duplex steels, the lowest i_{corr} belongs to 2304 with a value of 2.05E-07 A/cm^2 at 25°C. These were comparable values, with duplex 316LN having the slightly lower i_{corr}. Low i_{corr} values generally translate to lower corrosion rates.

Both the anodic (β_a) and cathodic (β_c) Tafel slopes of each alloy were found based on the experimental cyclic potentiodynamic polarization curves obtained. Generally, the lower value of Tafel slopes correlates to the higher corrosion rates as slight changes in potential can result in sever

change to the current density. The coordinating polarization curves for these calculation can be seen in **Figure 1**. Each material had varying anodic and cathodic Tafel slopes and are reported at 25°C, 45°C, and 65°C in **Table 2**.
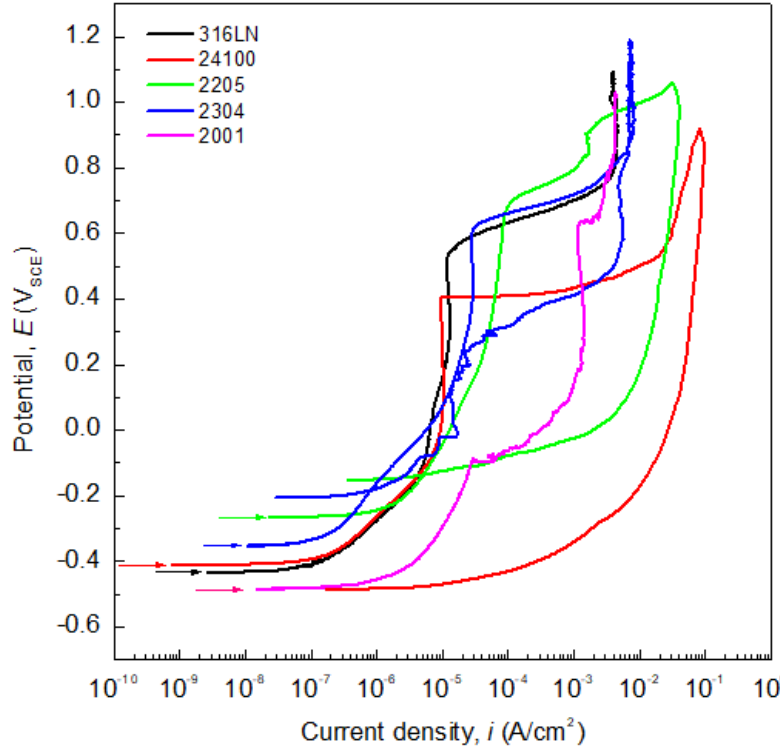

Figure 1 displays the cyclic potentiodynamic polarization curves for austenitic 316LN and 24100, along with duplex 2205, and lean duplex 2304 and 2001 at 25°C in simulated concrete pore solution containing [Cl⁻] = 1.0 M

Once the Tafel slopes were obtained for each alloy at each environmental condition, **Equation 8**, known as the Stern-Geary equation, can be used to find the Stern- Geary constant (B). These constants are also reported in **Table 2**.

$$B = \frac{\beta_a \, \beta_c}{2.303 \, (\beta_a + \beta_c)} \tag{8}$$

The Stern-Geary constant can be plugged into **Equations 9 and 10** to find the corresponding the electrochemical transfer coefficients of the anodic (α_a) and cathodic (α_c)

9

electrode reaction kinetics. In general, the higher values of electrochemical transfer coefficients correlates to faster kinetics.

$$\alpha_a = \frac{RT}{nF}\frac{1}{\beta_a} \tag{9}$$

$$\alpha_c = \frac{RT}{nF}\frac{1}{\beta_c} \tag{10}$$

Where R is the ideal gas constant, T is the system temperature in K, F is Faradays constant, and n is the number of electrons, which is 1 e$^-$ for this process.

Once the electrochemical transfer coefficient kinetics are understood for each alloy, the corresponding exchange current density ($i_{O,ORR}$) can be calculated with the intersection of the β_c and the equilibrium potential of oxygen (found at +240 mV$_{SCE}$).

When comparing exchange current densities of the austenitic, duplex, and lean duplex stainless steels, the duplex stainless steels exhibited higher values in all scenarios, with the exception of 2001 at 45°C and 65°C. Smaller exchange current densities are proportional to slower reaction kinetics, therefore better resistance to corrosion.

Table 2 CPP results including experimental Corrosion Potential, Corrosion Current Density, Pitting Potential, Passivation characteristics, and calculated exchange current density values with corresponding intermediate values.

Alloy	Temp. (°C)	E_{corr} V_{OCP}	i_{corr} $\mu A/cm^2$	E_{pit} mV_{OCP}	ΔE_{pass} mV	Repas. (yes/no)	β_a mV/dec	β_c mV/dec	B mV	$i_{0,ORR}$ nA/cm^2	α_a	α_c
316LN	25	-0.255	1.70E-07	550	250	N/A	0.2101	0.1695	0.0407	4.44E-04	0.1223	0.1516
	45	-0.419	1.04E-06	450	250	yes	0.1667	0.1823	0.0378	2.88E-03	0.1645	0.1504
	65	-0.433	1.46E-04	380	200	no	0.1386	0.1301	0.0291	1.85E-01	0.2102	0.224
24100	25	-0.409	2.45E-07	670	600	no	0.2269	0.1571	0.0403	6.89E-04	0.1132	0.1635
	45	-0.307	3.75E-07	400	300	no	0.2584	0.1317	0.0379	1.54E-03	0.1061	0.2082
	65	-0.267	1.45E-06	310	250	no	0.2653	0.1687	0.0448	3.80E-03	0.1098	0.1727
2205	25	-0.213	3.37E-06	750	500	yes	0.4807	0.2625	0.0737	6.26E-03	0.0534	0.0979
	45	-0.265	1.23E-05	700	450	no	1.2344	1.8105	0.3187	1.36E-02	0.0222	0.0151
	65	-0.302	3.74E-05	600	450	N/A	2.1541	1.4308	0.3733	3.94E-02	0.0135	0.0204
2304	25	-0.355	2.05E-07	680	400	yes	0.2741	0.1256	0.0374	7.47E-04	0.0937	0.2045
	45	-0.247	3.13E-06	610	300	yes	0.3908	0.2964	0.0732	5.41E-03	0.0701	0.0925
	65	-0.295	1.41E-05	470	300	yes	1.0347	0.932	0.2129	1.68E-02	0.0282	0.0313
2001	25	-0.238	2.43E-06	650	550	no	0.4725	0.5551	0.1108	3.26E-03	0.0544	0.0463
	45	-0.416	2.57E-07	630	500	no	0.6101	0.8619	0.1551	3.10E-04	0.0449	0.0318
	65	-0.417	3.28E-07	520	300	no	0.3318	0.1498	0.0448	9.70E-04	0.0878	0.1945

From this data, the E_{pit} can be drawn for each alloy. E_{pit} is a potential in which pitting initiates and varies with environmental factors such as temperature. In **Figure 1**, this potential is indicated by the area of the anodic region where current rapidly increases, with near static potential. This is where a pit initiated on the surface of the stainless steel. At 25°C, E_{pit} for the austenitic stainless steels, 316LN and 24100, were lower than those of the duplex and lean duplex stainless steels. This indicated ease of pit formation in the austenitic stainless steels when compared side by side to the three duplex stainless steels studied.

As temperature increases for any of the alloys, it is seen the E_{pit} decreases adjacently. Higher temperature, with other environmental factors staying constant results in likeliness of pit formation, in turn decreasing the corrosion resistance of the alloy.

4.2 Electrochemical Impedance Spectroscopy (EIS)

Each materials in all three environments were tested via non-destructive Electrochemical Impedance Spectroscopy. EIS testing allowed the production of Kramers-Kronig plot (**Figure 2**), Nyquist plots (**Figure 3**), and a Bode plot (**Figure 4**).

Kramers-Kronig (KK) transform plots are used to compare calculated real impedance from the imaginary impedance, and vice-versa. Both methods show good correlation, it can be concluded that the EIS data is robust. Below, **Figure 2** shows the KK transform for lean duplex 2001 at 25°C.
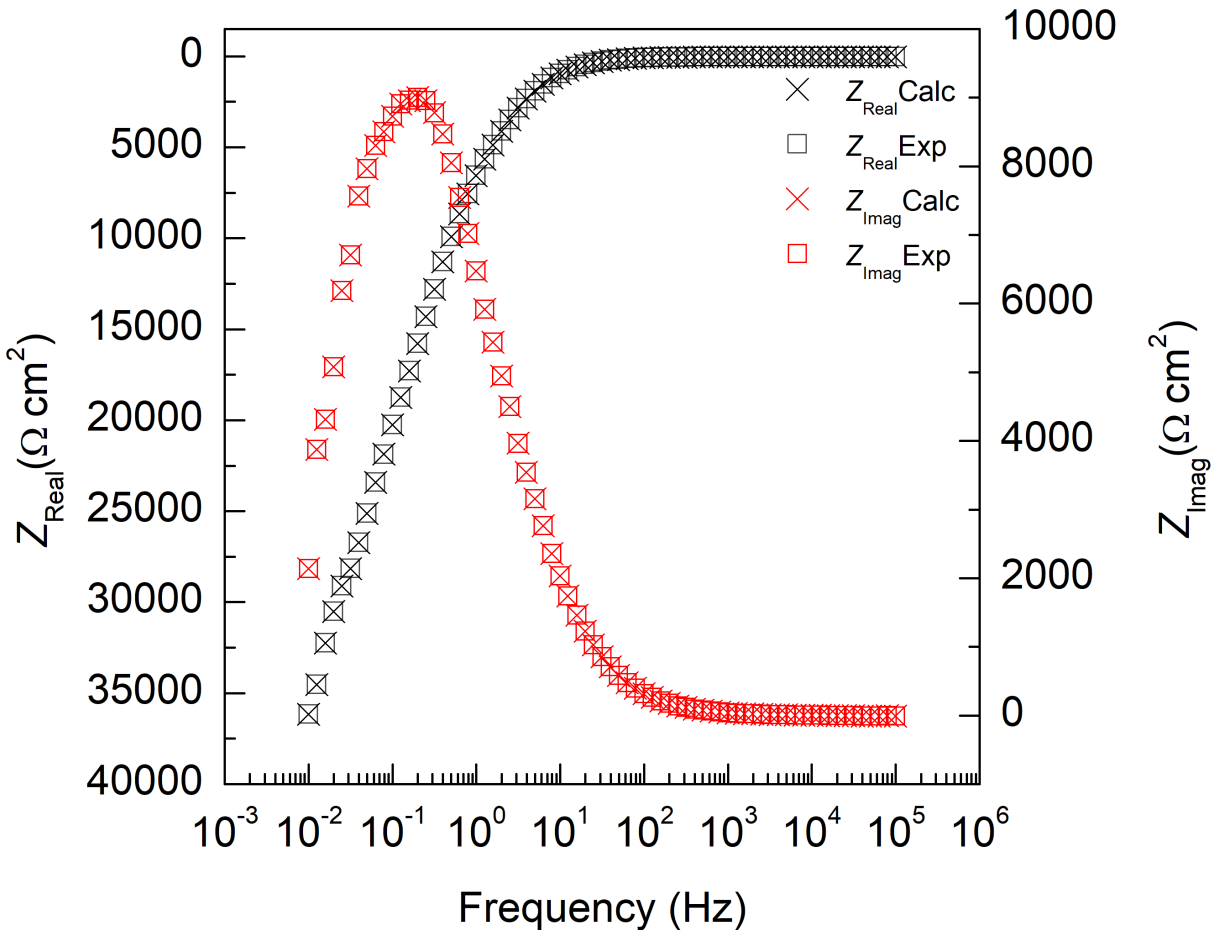
Figure 2 KK transform for lean duplex 2001 at 25ºC in simulated concrete pore solution containing [Cl⁻] = 1.0 M
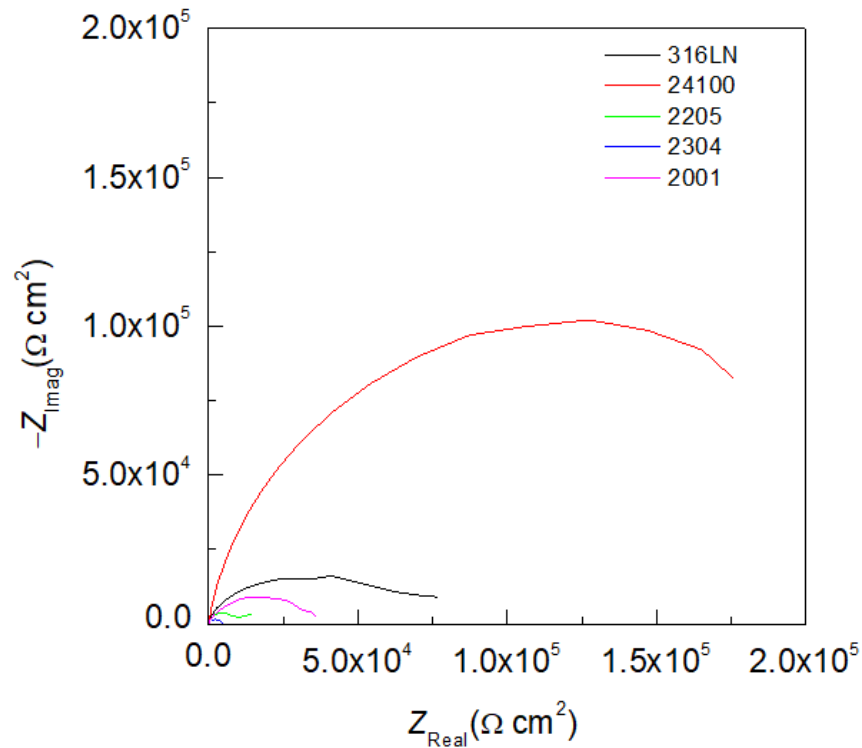

Figure 3 displays the Nyquist plot for Electrochemical Impedance Spectroscopy data obtained for austenitic 316LN and 24100, along with duplex 2205 and lean duplex 2304, and 2001 at 25ºC in simulated concrete pore solution containing [Cl⁻] = 1.0 M

In general, Nyquist plots can tell a bit of information based on the size and shape of the data sets obtained. Bigger impedance values, indicated by larger circles, indicate better resistance to corrosion. The largest impedance values exhibited by austenitic stainless steels was 24100. The largest impedance values exhibited by duplex and lean dupled stainless steels was 2001. Both austenitic stainless steels had higher impedance values than all of the duplex and lean duplex stainless steels, with lean duplex 2304 having the lowest impedance values of the group. In addition to the Nyquist plot, EIS testing can also formulate a Bode plot.
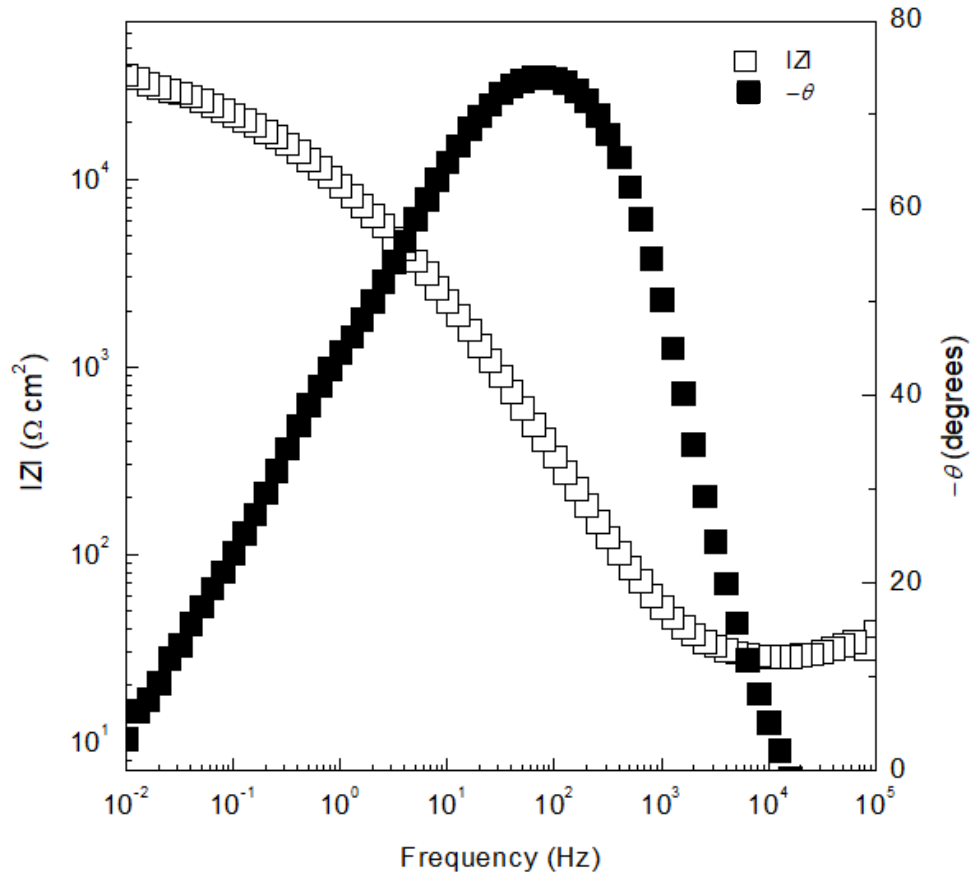
Figure 4 is a representative Bode plot for austenitic, duplex, and lean duplex stainless steels. This one in particular is for 2001 at 25°C in simulated concrete pore solution containing [Cl⁻] = 1.0 M

On a bode plot, there can be indication of two time constants, one indication a double layer and one indicating a passive layer. This is graphically shown by two changes in slope of the phase angle which represents the presence of two different relaxation processes.

For each bode plot, a few parameters can be drawn from it. In this study, the parameter of interest is the modulus of impedance(|Z|). This is indicated on the Bode by the highest impedance value recorded, usually at lowest frequencies. The modulus of impedance is highlighted for each alloy in **Table 3** below.

Table 3 summarizes the modulus of impedance for the austenitic, duplex, and lean duplex stainless steels recorded during EIS testing at 25°C, 45°C, and 65°C in simulated concrete pore solution containing [Cl⁻] = 1.0 M

EIS	Temp	316LN	24100	2205	2304	2001
|Z| Kohm /cm²	25°C	75.9	195.2	32.8	14.3	46.2
	45°C	6.6	96.6	15.1	4.2	35.6
	65°C	3.6	27	12.2	3.2	8.4

When comparing the modulus of impedance values for the alloys tested, the austenitic stainless steels reported higher values when tested at 25°C. When the temperature was raised to 65°C, the modulus of impedance tended to decrease, signifying less resistance to corrosion.

4.3 Cyclic Thermammetry (CT)

The main focus of this study is to observe the Critical Pitting Temperature for austenitic, duplex, and lean duplex stainless steels. After finding each stainless steel's pitting potential at 65°C via CPP, those observed potentials were used to run cyclic thermammetry for each sample. The CPT is distinguishable graphically where a temperature is reached and the current rapidly increase, sometimes even orders of magnitude. A total of five tests were ran where a critical pitting temperature was found for each alloy. Full testing results are shown in **Figure** 5 and are summarizes in **Table 4**.
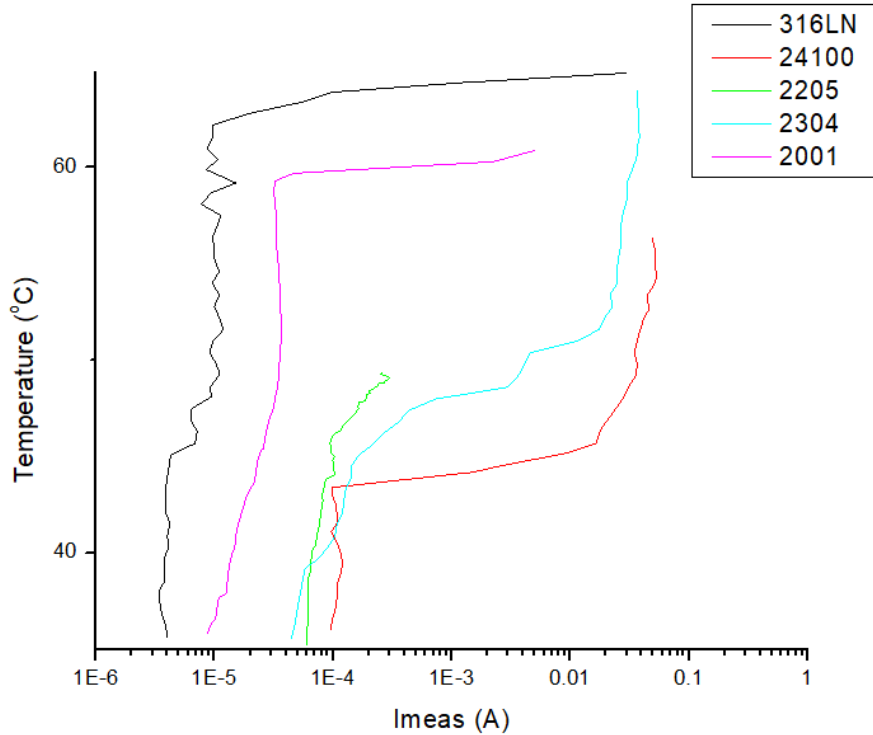
Figure 5 shows experimental cyclic thermammetry results for each alloy, with potential being unique to each alloy's pitting potential

Table 4 observed critical pitting temperature for the austenitic 316LN and 24100, duplex 2205, and lean duplex 2304 and 2001 in simulated concrete pore solution containing $[Cl^-] = 1.0$ M

Alloy	Critical Pitting Temperature (^{o}C)
316LN	63
24100	44
2205	46
2304	40
2001	59

When comparing the two austenitic stainless steels, 316LN exhibited much better corrosion resistance as its CPT was 19°C higher than that of 24100. Likewise, for the duple stees, there was a standout in 2001 as it had a 13°C increase when compared to 2205, and 19°C higher than 2304.

Overall, while one austenitic stainless steel, 316LN, performed the best, the other, 24100, performed second worst. Overall, the worst performing stainless steel when it comes to CPT was 2304. 316LN being on of the best performing, and 24100 almost being the worst performing aligns with the trend observed in pitting potential data. Higher pitting potential and higher critical pitting temperature characteristics correlate to better corrosion resistance.

4.4 Optical Microscopy (OM)

Upon completion of electrochemical testing, a variety of observation techniques were used to study the corrosion product and pits that were formed. The first of which was using an optical microscope. A pit from each of the five stainless steels were imaged and are shown in **Figure 6**.
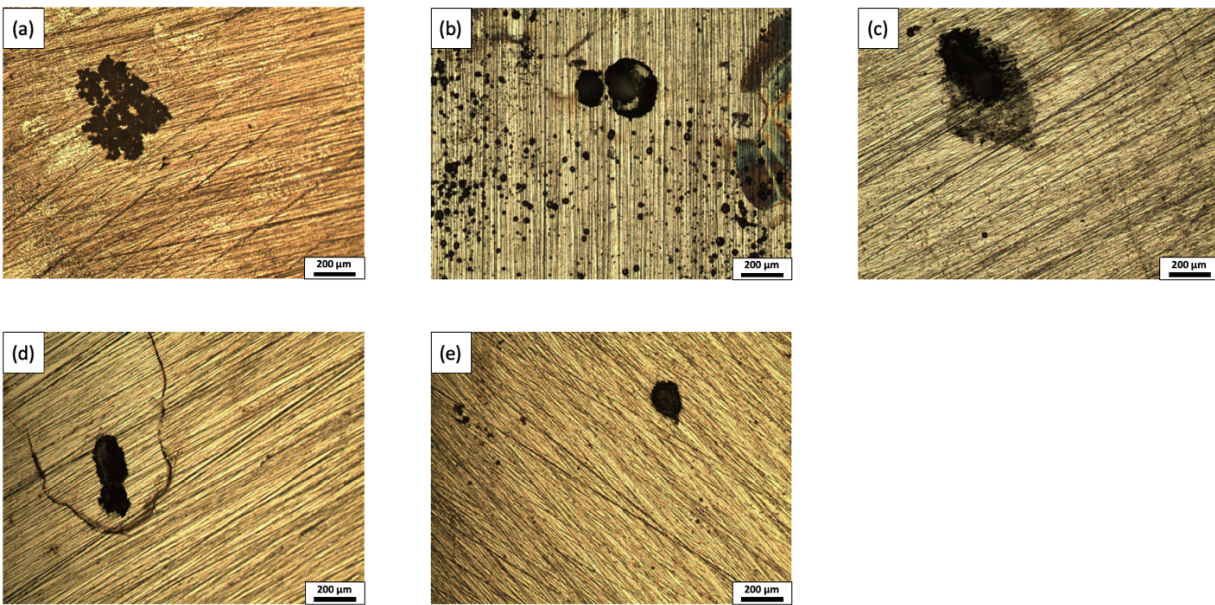

Figure 6 shows 10 X magnification Optical Microscopy imaging of pitting on lean duplex 2304 (a) and 2001 (b), duplex 2205 (c), and austenitic 316LN (d) and 24100 (e)

When observing the images taken by the optical microscope, there are differences in each stainless steel's pitting behaviour that can be observed. In general, it appears that the duplex and

lean duplex stainless steels experience a higher number of small pits that form and occasionally form clusters. For example, 2304 was seen to form pits of about 40 μm, that in turn cluster forming a larger pitting area up to 470 μm in width. A similar story can be told from 2001 and 2205 where the pits can grow up to 310 μm and 420 μm respectively in addition to an abundance of smaller pits forming across the surface.

When comparing this to the austenitic pitting tendencies, a distinct difference can be seen. The austenitic stainless steels appear to have a pit initiate in a distinct location and further propagate. 316LN pits got up to about 410 μm in length and about 150 μm in width. 24100 created a more circular pit with a diameter of about 230 μm.

4.5 Infinite Focus Microscopy (IFM)

In addition, the observing pit form and size, the depth is a telling parameter of how detrimental the pit is. Observing pit depth was done via Infinite Focus Microscopy (IFM). Imaging of two austenitic stainless steels, 316LN and 24100, lean duplex 2001, and duplex 2205, are show in **Figure 7**.
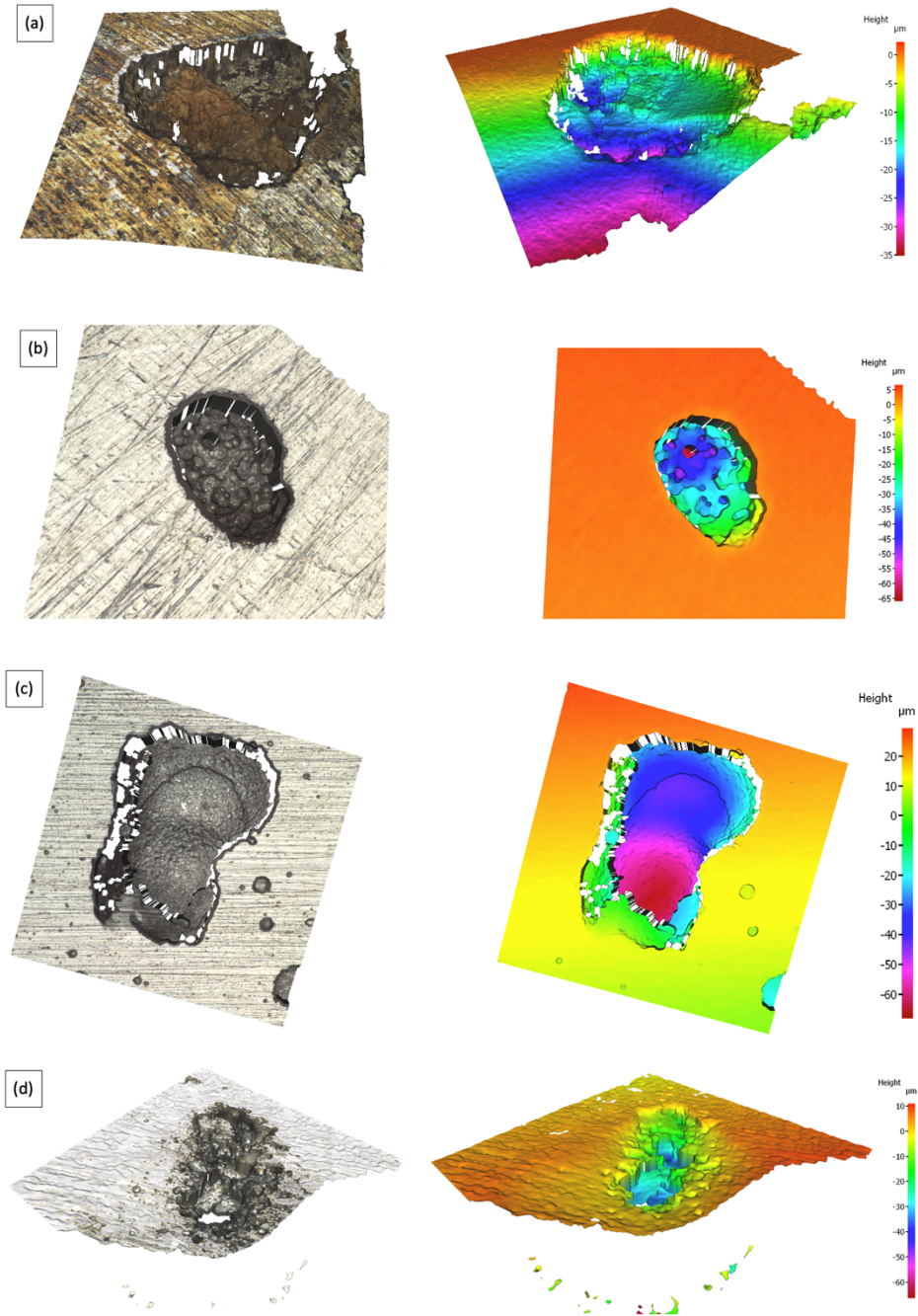
Figure 7 IFM imaging of austenitic 316LN (a), and 24100 (b), and lean duplex 2001 (c) and duplex 2205 (d)

A total of two austenitic, a duplex, and a lean duplex stainless steels were observed with infinite focus microscopy. When it comes to the austenitic stainless steels, they tended to form singular pits as opposed to clusters when looked at under the optical microscope. Austenitic 316LN

had a max pit depth of 30 μm with 24100 having pit depths up to 60 μm. Comparatively, lean duplex 2001 also approached the 60 μm pit depth benchmark with 2205 having max pit depths of around 40 μm. all samples were pitted electrochemically at 65°C at their potentiostatic pitting potential obtained from CPP.

4.6 Scanning Electron Microscopy (SEM)

When observing the pits from an imaging standpoint, sometimes the optical microscopy (OM) does not tell the whole story. This is where the use of a scanning electron microscope (SEM) is great for getting a higher resolution image of the pits, that can tell more of the story. An SEM was used to image the pits formed on the surface of austenitic 316LN and 24100 along with duplex 2205 and are displayed in **Figure 9.**
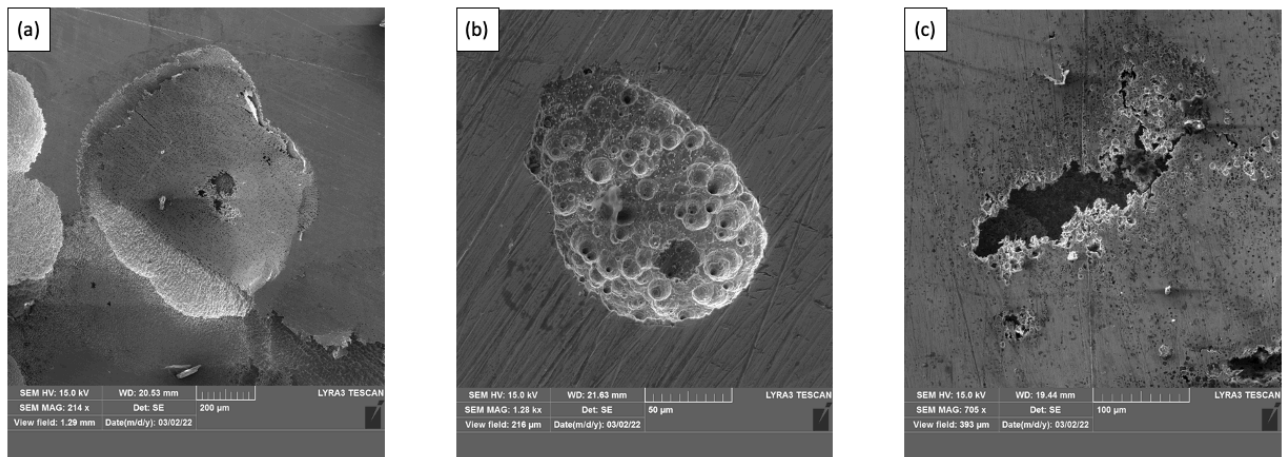

Figure 9 SEM imaging of pitting on austenitic 316LN (a), 24100 (b), and duplex 2205 (c)

As intended, the SEM gave a much better image of the pits included in 316LN, 24100, and 2205. Magnification of 214x shows 316LN as expected, with on large pit formed and propagated. However, a 1,280x magnification of the pit formed on 24100 tells a whole different story. Initially, the OM hinted the pit on austenitic 24100 was one large pit that grew and

20

propagated. The SEM revealed that is not necessarily the case. While one large pit outlines the corrosion, an abundance of micro-pits formed inside. These micro-pits show diameters of as small as 4 μm, much smaller than the initial pit size obtained from the optical microscopy. Similarly, duplex 2205 also saw an abundance of smaller pits, that clustered to form a larger pit. Pit in the 2205 grew as small as 3 μm and clustered to create a pit up to 250 μm.

5. Design Considerations

When it comes to building the world's infrastructure, concrete plays a major role. Concrete is a cheap, durable, and strong option that is resistant to extreme heat and accelerated degradation. With its extreme hardness and likeliness to experience shrinkage when it sets due to water evaporation, there is a lot of stress build up in concrete, which is nearly unavoidable. This is where the concept of reinforcing concrete comes into play.

Adding steel rebar into the matrix of concrete adds to the overall strength of the structure. The issue with this method of reinforcement is the threat of corrosion. Due to the high pH nature of concrete, carbonates are likely to form within the concrete. This, in addition to the leaching of chlorides through the concrete matrix, can lead to corrosion of the reinforcing steel in the concrete. When the iron oxidizes, the corrosion product always takes up more volume than the pure metal. Below in **Figure 10**, the relative volume of each corrosion product is compared to pure iron.
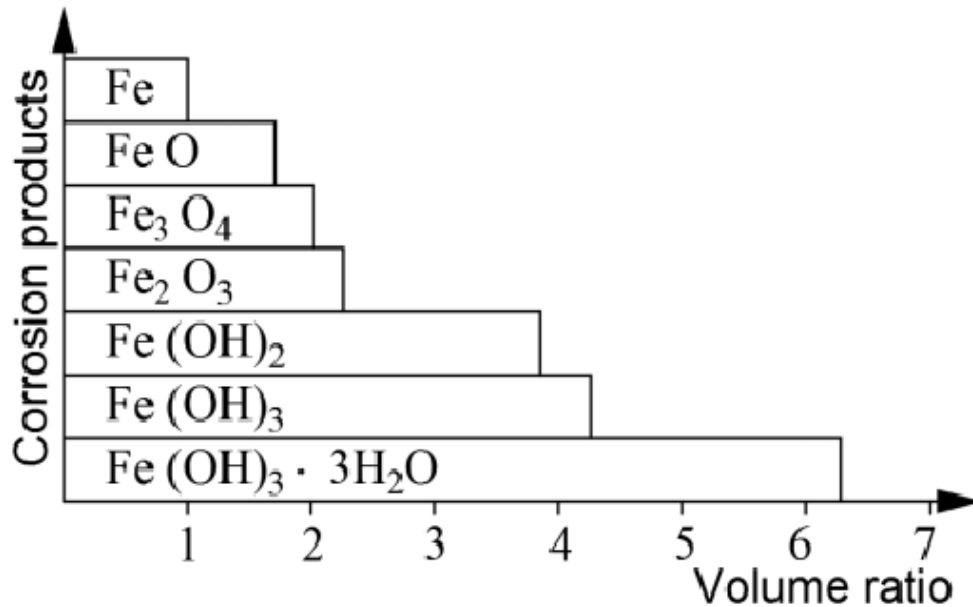
Figure 10 relative volume of iron oxide and iron hydroxide variants compared to pure iron.

Once concrete sets, it adopts a very rigid structure. If corrosion product forms on the surface of the steel, the added volume within the matrix will add extreme stresses to the structure. Once this corrosion begins to occur, a phenomenon known as spallation begins to happen which is the separation of the concrete from the reinforcement rebar. This leads to cracking and the eventual failure of the structure.

To prevent this, it is optimal to mitigate the corrosion of the reinforcements. This can be done via material selection, such as using stainless steel instead of carbon steel, or even by implementing a coating system to the carbon steel. Stainless steel, as previously mentioned, will mainly experience pitting corrosion. This localized corrosion will result is much less corrosion product, in turn reducing spallation. As carbon steel rebars will experience uniform corrosion, much more corrosion product can be expected, resulting in greater chance of failure.

5.1 Cost

When it comes to corrosion mitigation strategies for reinforcing steel in concrete, a popular method is via material selection. Carbon steel is popularly used as it is strong, and relatively cheap compared to stainless steels. Stainless steels require the presence of chromium to help improve corrosion resistance. This addition to composition increases the cost of the material and generally decreases the strength of the material. None the less, austenitic, duplex, and lean duplex stainless steels have been research as a material alternative. Carbon steel can cost around $500 per ton [8], whereas select stainless steels can cost four to five times as much, depending on the chromium and other alloying element composition within the steel. Taking that another step further, 304 stainless steel can cost upwards of $3,000 per ton.

In designing a reinforced concrete system, it is critical to fully understand the corrosion properties of your material option as paying a lot for a superalloy may not be necessary if proper mitigation can be handled otherwise. Consistently having to replace failed or corroded structures also incurs and incredible amount of costs over time, so a stress on service life is important in design consideration.

5.2 Safety

Designing of a structure will always have cost implications associated with it, but often times there is much more to be considered. One of these parameters is the safety of individuals that can be put at risk with the failure of a structure. Concrete is often used to support extremely heavy and load bearing structure, which would lead to catastrophe upon failure.

In June 2021, there was a tragedy that occurred in Miami, Florida. The South side of Chaplain Towers, and apartment complex, suddenly collapsed. This failure destroyed about half

of the 135 units within the complex, and importunely claimed the lives of 98 individuals. This building was supported by carbon steel reinforced concrete. An image of the aftermath can be seen in **Figure 11** below.

Figure 11 the collapsed South Chaplain Tower [20]

An in-depth investigation took place in hopes to find the cause of the collapse. Upon investigation, it was discovered that there was severe corrosion in the steel reinforced concrete around where the column met the foundry. The southside, being the seaside of the building, likely had leached chlorides from the nearby seawater. Prolonged exposure to chlorides and moisture led to sever corrosion of the steel reinforcements.

Further design consideration of this possibility could have saved the lives of nearly 100 people. Proper maintains was not maintained either. Had the reinforcements been designed with corrosion in mind, this degradation could have been delayed enough for proper maintenance to be

done. The use of austenitic or duplex stainless steels would have dramatically decreased the odds this tragic event.

The tragedies do not stop there however. One other specific case is the Fern Hollow Bridge Collapse in Pittsburgh that occurred in 2022. This failure was assessed by Dr. Hota, who is the director of Constructed Facilities Center at West Virginia University, and was found to injure 10 people [21]. This could have been much worse. The failure was found to be a result of corrosion and fatigue.

6. CONCLUSIONS

After testing the critical pitting temperature behavior of austenitic, duplex, and lean duplex stainless steels in simulated concrete pore solution contaminated with 1.0M NaCl, the following conclusions can be drawn.

When observing the pitting potential of various austenitic, duplex, and lean duplex stainless steels, the duplex and lean duplex stainless steels consistently exhibited higher pitting potentials at 25°C when compared to the austenitic stainless steels. A higher pitting potential is an indication of better resistance to corrosion, as it takes more polarization away from the open circuit potential for pitting to initiate. When comparing the same alloys based on exchange current densities, the majority of the results signified that the duplex and lean duplex stainless steels showed higher exchange current densities. This correlated to higher corrosion rates once the pitting is initiated.

Looking at EIS data, an important parameter to consider is the modulus of impedance ($|Z|$). The higher the $|Z|$, the better resistance to corrosion. Between the two austenitic stainless steels

studied, 24100 showed a higher |Z| of 195.2 Kohm/cm^2 at 25°C. For the duplex and lean duplex stainless steels, lean duplex 2001 exhibited the highest |Z| of 36.5 Kohm/cm^2 at 25°C.

When comparing the austenitic, duplex, and lean duplex steels in terms of CPT, the results varied. On average, the three classes of stainless steels performed about the same. For the austenitic stainless steels, 316LN outperformed 24100 with a CPT of 63°C, which was 19°C higher than that of 24100. For the lean duplex steels, 2001 had a CPT of 59°C, which was 19°C higher than 2304, and 13°C higher than duplex 2205. Overall, 316LN showed the highest CPT of 63°C, with 2304 having the lowest of 40°C. The critical pitting temperature is another parameter which indicated the likeliness of a pit to form on a given materials surface. Materials with higher CPT can withstand higher temperatures before pitting begins to occur.

Observation techniques allowed for characterization of the pits formed. The deepest pits formed in 24100 and 2001 which were around 60 μm in depth. While 316LN formed one large pit, the duplex and lean duplex stainless steels formed many smaller pits in colonies. Uniquely, 24100 formed what appeared to be one large pit, but was actually made up of many micro-pits.

7. REFERENCES

[1] E. McCafferty, *Introduction to Corrosion Sciences,* Springer Science + Business Media, LLC 2010

[2] M.F. Hurley, J.R. Scully, *Threshold Chloride Concentration of Selected Corrosion- Resistant Rebar Material Compared to Carbon Steel,* pg. 892-904, NACE International 2006

[3] N. Ebrahhimi, M. Momeni, A. Kosari, M. Zakeri, M.H. Moayed, *A Comparative Study of Critical Pitting Temperature (CPT) of Stainless Steel by Electrochemical Impedance Spectroscopy (EIS), Potentiodynamic and Potentiostatic Techniques,* Corrosion Science 96-102, 2012

[4] H. Hoseinpoor, M. Momeni, M.H. Moayed, A. Davoodi, *EIS Assessment of Critical Pitting Temperature of 2205 Duplex Stainless Steel in Acidified Ferric Chloride Solution,* Corrosion Science 197-204, 2014

[5] H. Ke, *Application of the Chloride Susceptibility Index to Study the Effects od Ni, Cr, Mn, and Mo on the Passivation of Stainless Steel,* Journal of the Electrochemical Society, 2020

[6] D. M. Bastidas, *What is Critical Pitting Corrosion Temperature and Critical Crevice Corrosion Temperature ,*The University of Akron 2020

[7] ASTM G150-18, *Standard Test Method for Electrochemical Critical Pitting Temperature Testing of Stainless Steels and Related Alloys,* ASTM International, West Conshohocken, PA, 2018

[8] *What are Costs of Stainless Steels – Price,* Material Properties, 2022

[9] P. Knyziak, P. M. Bieranowski, J. Krentowski, Impact of Corrosion Processes in the Basement Level on the Durability of the Construction of Large- Panel Buildings, MATEC Web of Conferences, 2017

[10] Martin, U.; Ress, J.; Bosch, J.; Bastidas, D.M. Stress corrosion cracking mechanism of AISI 316LN stainless steel rebars in chloride contaminated concrete pore solution using the slow strain rate technique. Electrochim. Acta 2020, 335, 135565, doi:10.1016/j.electacta.2019.135565.

[11] Feng, X.; Lu, X.; Zuo, Y.; Chen, D. The passive behaviour of 304 stainless steels in saturated calcium hydroxide solution under different deformation. Corros. Sci. 2014, 82, 347 355, doi:10.1016/j.corsci.2014.01.039.

[12] Feng, X.; Zhang, X.; Xu, Y.; Shi, R.; Lu, X.; Zhang, L.; Zhang, J.; Chen, D. Corrosion behavior of deformed low-nickel stainless steel in groundwater solution. Eng. Fail. Anal. 2019, 98, 49–57, doi:10.1016/j.engfailanal.2019.01.073.

[13] Moser, R.D.; Singh, P.M.; Kahn, L.F.; Kurtis, K.E.; Niño, D.G.; McClelland, Z.B. Crevice corrosion and environmentally assisted cracking of high-strength duplex stainless steels in simulated concrete pore solutions. Constr. Build. Mater. 2019, 203, 366–376, doi:10.1016/j.conbuildmat.2019.01.082.

[14] Zhang, W.; François, R.; Cai, Y.; Charron, J.-P.; Yu, L. Influence of artificial cracks and interfacial defects on the corrosion behavior of steel in concrete during corrosion initiation under

a chloride environment. Constr. Build. Mater. 2020, 253, 119165, doi:10.1016/j.conbuildmat.2020.119165.

[13] Mahajanam, S.P. V; Case, R.P.; Rincon, H.E.; Mcintyre, D.R.; Joosten, M.W.; Gjesdal, S.; Monsen, H. CORROSION SCIENCE SECTION Study of Environmentally Assisted Cracking of Duplex Stainless Steels as a Result of the Presence of Sigma Phase; 2011;

[14] S. Fajardo, D.M. Bastidas, M.P. Ryan, M. Criado, D.S. McPhail, J.M. Bastidas, Low- nickel stainless steel passive film in simulated concrete pore solution: A SIMS study, Appl. Surf. Sci. 256 (2010) 6139–6143, https://doi.org/10.1016/j. apsusc.2010.03.140.

[15] M.F. Hurley, J.R. Scully, Threshold chloride concentrations of selected corrosion-resistant rebar materials compared to carbon steel, Corrosion 62 (2006) 892–904

[16] M. Y. Ho, J. Geddes, E. Barmatov, L. Crawford, and T. Hughes, *Corros. Sci.*, **137**, 43–52 (2018). https://doi.org/10.1016/j.corsci.2018.03.022.

[17] X. Li, K. H. Lo, C. T. Kwok, Y. F. Sun, and K. K. Lai, *Constr. Build. Mater.*, **174**, 150–158 (2018). https://doi.org/10.1016/j.conbuildmat.2018.04.110.

[18] C. R. de Farias Azevedo, H. Boschetti Pereira, S. Wolynec, and A. F. Padilha, *Eng. Fail. Anal.*, **97**, 161–188 (2019). https://doi.org/10.1016/j.engfailanal.2018.12.009.

[19] Gamry, *Getting Started with Electrochemical Corrosion Measurements,* Gamry Instruments, Warminster PA

[20] I. Block, *Report on Collapsed Miami Building Warned of "Abundant Cracking" in its*

Concrete, Dezeen 2021

[21] E. Blazina and S. Hamill, *Pittsburgh Post-Gazette* https://www.post-gazette.com/news/transportation/2022/02/07/National-Transportation-Safety-Board-Fern-Hollow-bridge-collapse-preliminary-report-cause-pittsburgh/stories/202202070093.

[22] U. Martin, J. Bosch, J. Ress, D.M. Bastidas, Long-term stability and electronic properties of passive film of lean-duplex stainless steel rebars in chloride containing mortar, *Const. Build. Mater.* 291 (2021) 123319.

[23] ASTM G61-86, *Standard Test Method for Conducting Cyclic Potentiodynamic Polarization Measurements for Localized Corrosion Succeptibility of Iron-, Nickle-, or Cobalt-Based Alloys,* ASTM International, West Conshohocken, PA, 2018

[24] U. Martin, J. Ress, J. Bosch, D.M. Bastidas, Stress corrosion cracking mechanism of AISI 316LN stainless steel rebars in chloride contaminated concrete pore solution using the slow strain rate technique. *JOURNAL: Electrochim. Acta* 335 (2020) 135565.